Neuron, Vol. 31, 115–130, July 19, 2001, Copyright ©2001 by Cell Press

Regulation of Dendritic Spine Morphology and Synaptic Function by Shank and Homer

Carlo Sala,[1] Valentin Piëch,[1] Nathan R. Wilson,[2] Maria Passafaro,[1] Guosong Liu,[2] and Morgan Sheng[1,2,3]
[1] Howard Hughes Medical Institute and Department of Neurobiology
Massachusetts General Hospital and Harvard Medical School
Boston, Massachusetts 02114
[2] Center for Learning and Memory
RIKEN-MIT Neuroscience Research Center
Department of Brain and Cognitive Sciences
Massachusetts Institute of Technology
Cambridge, Massachusetts 02139

Summary

The Shank family of proteins interacts with NMDA receptor and metabotropic glutamate receptor complexes in the postsynaptic density (PSD). Targeted to the PSD by a PDZ-dependent mechanism, Shank promotes the maturation of dendritic spines and the enlargement of spine heads via its ability to recruit Homer to postsynaptic sites. Shank and Homer cooperate to induce accumulation of IP3 receptors in dendritic spines and formation of putative multisynapse spines. In addition, postsynaptic expression of Shank enhances presynaptic function, as measured by increased minifrequency and FM4-64 uptake. These data suggest a central role for the Shank scaffold in the structural and functional organization of the dendritic spine and synaptic junction.

Introduction

The postsynaptic membrane of central excitatory synapses is characterized by an electron-dense thickening known as the postsynaptic density (PSD), which contains glutamate receptors and other membrane proteins anchored in a matrix of cytoskeletal and signaling molecules (Garner et al., 2000; Kennedy, 1997; Sheng and Pak, 2000; Ziff, 1997). The Shank family of proteins (also known as ProSAP, SSTRIP, cortBP, Synamon, and Spank) are core components of the PSD and share a domain organization consisting of ankyrin repeats near the N terminus, followed by SH3 domain, PDZ domain, proline-rich region, and a SAM domain at the C terminus (Boeckers et al., 1999a; Du et al., 1998; Ehlers, 1999; Lim et al., 1999; Naisbitt et al., 1999; Sheng and Kim, 2000; Tu et al., 1999; Yao et al., 1999; Zitzer et al., 1999a). Complex alternative splicing of three Shank genes generates multiple isoforms of Shank proteins (Boeckers et al., 1999a; Lim et al., 1999).

Consistent with a scaffolding function of Shank polypeptides, multiple protein interactions mediated by Shank have been identified. The PDZ domain binds to the guanylate kinase-associated protein (GKAP) family of PSD-95 binding proteins, thereby linking Shank to the *N*-methyl-d-aspartate (NMDA) receptor/PSD-95 complex (Boeckers et al., 1999b; Naisbitt et al., 1999; Tu et al., 1999). In addition, the PDZ domain interacts with somatostatin receptors and the calcium-independent α-latrotoxin receptor (Kreienkamp et al., 2000; Tobaben et al., 2000; Zitzer et al., 1999a, 1999b). Two distinct proline-based motifs within the proline-rich region of Shank form the binding sites for cortactin, an actin regulatory protein, and for Homer, which also binds group 1 metabotropic glutamate receptors and inositol-1,4,5-trisphosphate (IP3) receptors (Naisbitt et al., 1999; Tu et al., 1999; Xiao et al., 2000). Through its interactions with GKAP and Homer, Shank has the potential to link together the NMDA receptor and metabotropic glutamate receptor complexes in the postsynaptic specialization.

By quantitative immunogold localization, Shank is concentrated in the deep part (near the cytoplasmic face) of the PSD; in comparison, PSD-95 lies very close to the postsynaptic membrane (Valtschanoff and Weinberg, 2001). Thus, Shank may play a role at the interface between the PSD and the postsynaptic cytoplasm and cytoskeleton. Consistent with this idea is the interaction of Shank with cortactin, an actin binding protein that translocates to the cortical cytoskeleton in response to extracellular stimuli (Naisbitt et al., 1999; Weed et al., 1998).

Excitatory synapses (and PSDs) in the central nervous system (CNS) are found predominantly on dendritic spines, specialized structures that protrude from dendritic shafts. Mature spines typically have a "mushroom" shape characterized by a thin neck and a bulbous head on which synapses usually form. Dendritic spines are semiautonomous compartments that often contain smooth endoplasmic reticulum (SER) and protein translational machinery (Harris, 1999a; Harris and Kater, 1994). The predominant cytoskeleton of spines is F-actin, and spines undergo continual actin-based motility over a time frame of seconds to minutes (Fischer et al., 1998; Matus et al., 2000).

On a longer time scale, the morphology of dendritic spines appears to change in response to many factors, including learning, age, hormones, and disease (Bailey and Kandel, 1993; Harris and Kater, 1994; Horner, 1993). This morphological plasticity has led to the idea that long-term memory may be encoded, at least in part, by alterations in spine structure and associated synaptic connections (Calverley and Jones, 1990; Muller et al., 2000). For instance, long-term potentiation (LTP) has been correlated with altered spine size (Fifkova and Van Harreveld, 1977; Hosokawa et al., 1995), spine bifurcation (Rusakov et al., 1997), and the emergence of new spines (Engert and Bonhoeffer, 1999; Maletic-Savatic et al., 1999), as well as with increased synapse size (Desmond and Levy, 1988) and perforation of the PSD (Toni et al., 1999). Little is known, however, about the molecular mechanisms that determine the structure of dendritic spines and their associated synapses, particularly with respect to the role of PSD proteins.

[3] Correspondence: msheng@mit.edu

Since it lies at the cytoplasmic face of the PSD and interacts with cortactin as well as glutamate receptor complexes, Shank seems a good candidate to link synaptic activity to regulation of the postsynaptic cytoskeleton. Here, we report that Shank promotes the maturation of dendritic spines and the selective enlargement of spine heads via a mechanism that depends on the postsynaptic recruitment of Homer. Accompanying the spine enlargement, Shank and Homer cause accumulation of IP3 receptors and other PSD proteins in dendritic spines and induce the formation of putative multisynapse spines. Electrophysiologically, the major effect of postsynaptic Shank is to enhance presynaptic function. These pleomorphic effects reveal a central role for the Shank scaffold in the structural and functional organization of the dendritic spine and synapse.

Results

Shank1 Promotes Spine Maturation and Spine Head Enlargement

To obtain insights into the function of Shank, we looked for "gain-of-function" phenotypes in cultured hippocampal neurons transfected with wild-type Shank (Figure 1). Two splice variants of Shank1 were initially tested: the "full-length" Shank1A and Shank1B (which lacks the SAM domain and part of the proline-rich region) (see below and Lim et al., 1999). Green fluorescent protein (GFP) was cotransfected with the Shank constructs to fill the cells and to outline the morphology of transfected neurons.

Neurons transfected with Shank1B showed a striking enlargement of dendritic spines, as visualized by cotransfected GFP (Figures 1A and 1B). The spine-promoting effect was seen in young and mature neurons. At days in vitro 7 (DIV7), control neurons showed mostly filopodia-like outgrowths (thin processes lacking a head; Figures 1Aa and 1Ac, arrows). In contrast, DIV7 neurons transfected with Shank1B showed shorter dendritic spines with well-developed spine heads on thin spine necks (mushroom-like spines; Figures 1Ab and 1Ad, arrowheads). Thus, in immature neurons, Shank1B overexpression promoted the morphological maturation of spines. By DIV18, control neurons have developed a higher density of spines, some of which are mushroom shaped (Figures 1Ae and 1Ag, arrows). However, DIV18 neurons transfected with Shank1B showed much more prominent dendritic spines, virtually all of which were mushroom shaped, with spine heads larger than control neurons (Figures 1Af and 1Ah, arrowheads). Transfection of Shank1A or Shank3 (a closely related gene) had the same effect on dendritic spine morphology as Shank1B (data not shown). Shank overexpression had no obvious effect on dendritic shaft structure, dendritic branching pattern, or on axons, thus, the morphological effect of Shank was selective for dendritic spines (Figure 1B). Exogenous Shank1B protein (stained by HA antibodies) localized specifically in dendritic spines of transfected neurons (Figures 1Ba1 and 1Bc1).

To quantify the effect of Shank on spine morphology, we measured the length of spines and the width of spine heads from stacked z series confocal images, using the coexpressed GFP to outline the shape and dimensions of dendritic spines (Figure 2 and Table 1). Although the extent of GFP fluorescence does not necessarily report spine size accurately in the absolute quantitative sense, these GFP measurements are valid for showing relative changes in the length and/or diameter of spines. The frequency distributions of spine length and width for individual dendritic spines were plotted on three-dimensional graphs (Figures 2A and 2B; at least 600 spines measured for each condition). Control DIV7 neurons transfected with GFP alone showed dendritic protrusions of highly variable length (many >1.5 μm long) with poorly developed spine heads (diameter at spine tip mostly <0.6 μm) (Figure 2A, upper). This graph reflects the heterogeneous filopodia-like processes exhibited by immature DIV7 neurons. In contrast, same-age neurons transfected with Shank1B had shorter spines (mostly between 0.7 and 1.5 μm in length) with larger diameter spine heads (peak of distribution at 0.6–0.9 μm) (Figure 2A, lower). The 3D representation of DIV7 Shank-expressing spines shows an upward shift along the *y* axis (width of spine head) and a narrower spread in the *x* axis (length of spine), reflecting the greater uniformity of dendritic spine length in the Shank-expressing neurons. Expressed numerically, the mean length of dendritic spines was reduced in Shank1B-transfected DIV7 neurons (from 1.74 μm to 1.54 μm; $p < 0.05$, Student's t test), while the mean diameter of the spine head increased (from 0.52 to 0.78 μm; $p < 0.05$) (see Table 1). Thus, in immature neurons (DIV7), Shank induces the appearance of mushroom-shaped spines.

Later in development (DIV18), control GFP neurons already show many dendritic spines with a well-defined head (Figures 1Ae and 1Ag). Detailed quantitation revealed that the frequency distribution of spine length and width of control DIV18 neurons was similar to DIV7 neurons transfected with Shank1B (compare Figure 2B, upper, with Figure 2A, lower). However, compared with DIV18 neurons expressing GFP alone, DIV18 neurons expressing GFP + Shank1B showed an increase in spine head diameter (upward shift of 0.4 μm) and a more modest increase in spine length (rightward shift of 0.2 μm) (Figure 2B, compare upper and lower panels). Despite this upward and rightward shift in response to Shank overexpression, the overall spread of the length/width distribution (shape of the 3D representation) changed little (Figure 2B), suggesting that Shank exerted a relatively uniform effect on most or all spines. In cumulative frequency plots, Shank1B transfection induced a rightward shift in spine head diameter in DIV7 and DIV18 neurons (Figures 2C and 2D). The parallel rightward shift (0.3–0.4 μm) in DIV18 neurons implies that a wide range of spines rather than a restricted subpopulation is modified by Shank. The linear density of spines on dendrites was not changed significantly by Shank overexpression. We conclude that overexpression of Shank in developing neurons promotes the maturation of mushroom spines and, in older neurons, causes enlargement particularly of the spine head.

Synaptic Targeting of Shank

Since the postsynaptic localization of Shank may be required for its effect on spine morphology, we first analyzed the molecular determinants of Shank targeting

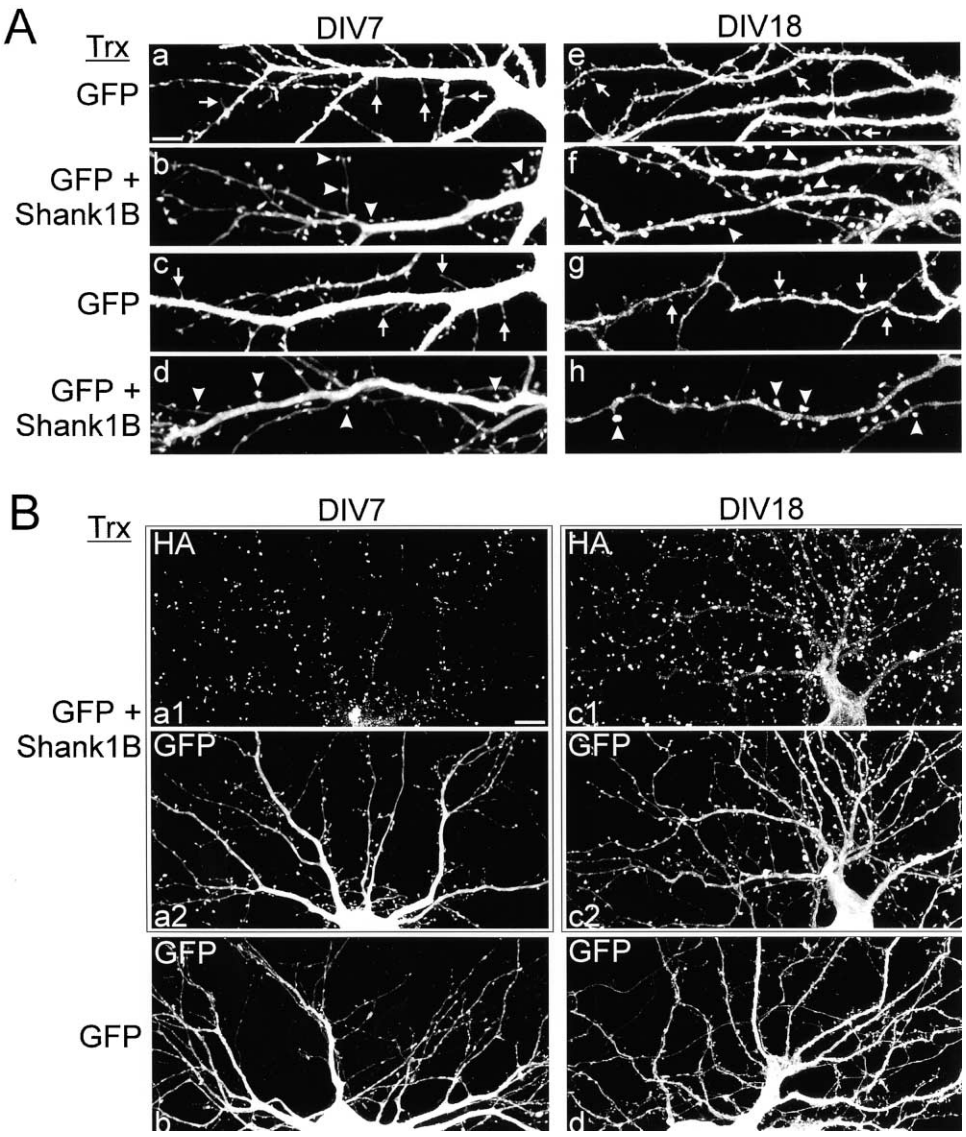

Figure 1. Shank1 Promotes Development and Enlargement of Mushroom Spines

High-density hippocampal neurons were transfected ("Trx") with GFP alone or with HA-Shank1B and GFP at DIV4 and DIV12 and stained for GFP and HA at DIV7 and DIV18, respectively. (A) Examples of dendrites from transfected neurons at DIV7 (left) and DIV18 (right). Only the GFP channel is shown in all panels to outline dendrite morphology. Compared with spines of control GFP-transfected neurons (arrows), spines of Shank1B-transfected neurons have more prominent mushroom shape (arrowheads) at DIV7 and larger spine heads (arrowheads) at DIV18. Scale bar, 5 μM. (B) Lower magnification views of transfected neurons stained at DIV7 (left) or DIV18 (right). Paired panels ([Ba1]/[Ba2] and [Bc1]/[Bc2]) are double-label images of GFP and HA-Shank1B in the same neuron, as indicated in each panel. GFP images show that Shank1B promotes spine enlargement throughout the dendrites (Ba2 and Bc2) but does not affect the overall morphology of neurons compared with control GFP-transfected neurons (Bb and Bd). The exogenous HA-Shank1B protein, revealed by HA antibodies (Ba1 and Bc1), is mainly localized to dendritic spines of DIV7 (Ba1) and DIV18 neurons (Bc1). Scale bar, 10 μM.

to dendritic spines. A series of deletion and point mutants of Shank1 (HA-tagged at the N terminus) were transfected in hippocampal neurons and their subcellular distribution determined by HA immunostaining (Figure 3). Wild-type HA-Shank1A accumulated in numerous puncta flanking the main shaft of dendrites (characteristic of localization in dendritic spines) (Figure 3Ba1). These puncta colocalized with endogenous Bassoon, a presynaptic active zone protein (Figure 3Ba2) and with synaptophysin (data not shown), confirming that exogenous Shank1A is targeted to synapses like endogenous Shank (Naisbitt et al., 1999). A similar spiny/synaptic staining pattern was found for splice variant Shank1B and for the following Shank1 mutants: Shank1B(P1497L), (1-1440), (1-840), (577-1849), (577-1440), and (481-840) (Figures 3B and 3C). To obtain a numerical index of postsynaptic targeting, we measured the ratio of immunofluorescence intensity between the spine head and the dendritic shaft and found that the above constructs showed a spine/shaft ratio of >3 (Figure 3A).

Many of the deletion mutants of Shank1 failed to accumulate in dendritic spines after transfection in cultured

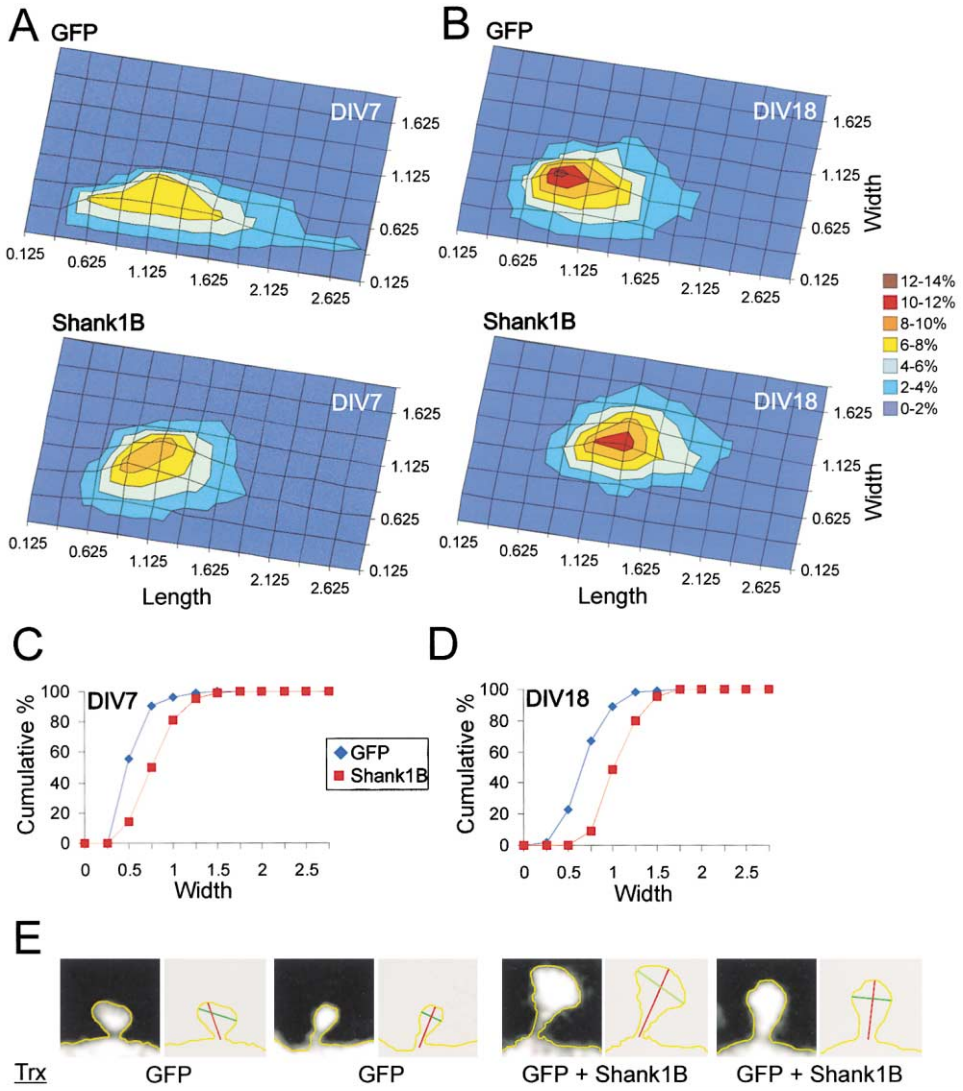

Figure 2. Quantitation of Shank1 Effects on Spine Morphology

(A and B) Three-dimensional graphs of the frequency distribution of spine length and spine head width in neurons transfected with GFP alone (upper graphs) or with GFP + Shank1B (lower graphs). (A) Data for neurons transfected at DIV4 and stained at DIV7. (B) Data for neurons transfected at DIV12 and stained at DIV18. The 3D graph displays the percentage of spines with a particular combination of length and width. The percentage refers to bins of 0.25 μm length and 0.25 μm width (grid size in the graph).

(C and D) Cumulative frequency plots of spine head width in neurons transfected with GFP alone (blue diamonds; n = 12 for DIV7, and n = 15 for DIV18) or with GFP + Shank1B (red squares; n = 10 for DIV7, and n = 16 for DIV18).

(E) Examples of spines from neurons transfected at DIV12 with GFP or with GFP + Shank1B, as indicated, and visualized for GFP at DIV18. The outline of the spine was manually traced (yellow line) from z series projection images such as these. Spine length (red line) and head width (green line) were computed using MetaMorph software.

neurons: (1-753), (753-1849), ΔSP, (577-840), (481-753), and (577-753). The staining pattern of these Shank mutants was relatively diffuse (Figure 3D), with spine/shaft ratios <2 (Figure 3A). One particular mutant [(1-618)] was even targeted preferentially to axons (Figure 3Dg1).

The smallest Shank construct tested that targeted efficiently to dendritic spines was Shank1(481-840) (Figure 3Cf; spine/shaft ratio = 3.8). Thus, the N-terminal region containing the ankyrin repeats and most of the proline-rich region of Shank1 are not required for synaptic targeting. A mutant lacking the SH3 and PDZ domains (ΔSP) failed to concentrate in spines (Figure 3Dc). However, the SH3 domain is dispensable for postsynaptic targeting, since deletion mutants (577-1849) and (577-1440), which lack the SH3 domain, were efficiently localized at synapses (Figures 3Cd and 3Ce). Deletion of the PDZ domain from mutant (577-1849) (spine/shaft ratio = 16.5) abolished synaptic localization [(753-1849), spine/shaft ratio = 0.7; Figure 3Db], highlighting the importance of the PDZ domain for synaptic targeting. Indeed, no construct lacking the PDZ domain showed specific accumulation in dendritic spines. However, neither the isolated PDZ domain (577-753) nor slightly bigger constructs including the SH3 domain (481-753) or flanking proline-rich region (577-840) were able to target to synapses (Figure 3D). Although these small constructs ex-

Table 1. Dendritic Spine Size in Neurons Overexpressing Shank and Homer

Age of Culture	Transfected with	Length (±SD) of Spine (μm)	Width (±SD) of Spine Head (μm)
DIV7	GFP	1.73 (±0.96)	0.55 (±0.20)
DIV7	GFP + Shank1B	1.59 (±1.21)[a]	0.79 (±0.25)[a]
DIV18	GFP	1.28 (±0.50)	0.68 (±0.25)
DIV18	GFP + Shank1B	1.48 (±0.45)[b]	1.05 (±0.25)[b]
DIV18	GFP + Shank1B + Homer1b	1.77 (±0.56)[b,c]	1.31 (±0.41)[b,c]
DIV18	GFP + Shank1B(P1497L)	1.14 (±0.39)[c]	0.61 (±0.19)[c]
DIV18	GFP + (1-1440)	1.20 (±0.47)[c]	0.56 (±0.17)[c]
DIV18	GFP + (481-840)	0.98 (±0.26)[b,c]	0.53 (±0.14)[b,c]
DIV18	GFP + Shank1BΔSP	1.22 (±0.47)[c]	0.57 (±0.16)[c]
DIV18	GFP + Homer1b	1.10 (±0.34)[c]	0.64 (±0.19)[c]

[a] Values statistically different ($p < 0.05$) from values obtained in neurons transfected with GFP at DIV7.
[b] Values statistically different ($p < 0.05$) from values obtained in neurons transfected with GFP at DIV18.
[c] Values statistically different ($p < 0.05$) from values obtained in neurons transfected with GFP + Shank1B.

pressed well in COS cells by immunoblotting and in neurons by immunostaining, we cannot be certain that they fold correctly.

In conclusion, the mutational analysis indicates that the PDZ domain of Shank is necessary but apparently not sufficient for targeting to postsynaptic sites. Additional flanking sequences are required on both sides of the PDZ domain—perhaps to allow proper folding of the PDZ domain or to mediate specific interactions needed for targeting. The importance of the Shank PDZ domain for targeting to postsynaptic sites is consistent with our previous finding that the C terminus of GKAP (which binds directly to Shank's PDZ) is involved in synaptic localization of Shank (Naisbitt et al., 1999).

Homer Binding and Synaptic Localization Required for Shank Effect on Spine Morphology

Having identified the determinants of synaptic targeting of Shank, we turned to the domain requirements for Shank-induced enlargement of spines. A subset of Shank1 constructs described in Figure 3 was transfected into hippocampal neurons with GFP and their effects on spine morphology compared to control cells transfected with GFP alone. Shank1B was at least as effective as Shank1A in promoting the growth of dendritic spines and was used as a "positive control" (Figures 4Ab1 and 4C). Since Shank1B lacks the putative cortactin binding site (see Figure 3A), this result suggests that cortactin is not involved in the Shank effect on spines. Deleting a further ~350 amino acids of the proline-rich region [giving rise to mutant (1-1440)] abolished the ability of Shank1 to induce spine enlargement (Figures 4Ac1, 4C, and 4D), even though Shank1(1-1440) targeted efficiently to spines (Figure 3). The Homer binding site (PPPLEFS) lies within the proline-rich region of Shank1 that is deleted in the (1-1440) mutant (Tu et al., 1999). Substitution of a critical proline residue (P1497) of the Homer binding motif [Shank1B(P1497L)] abolished the ability of Shank1B to increase spine width, even though the mutant localized efficiently in spines (Figures 4Ad1, 4Ad2, and 4C). These data indicate that Homer binding is essential for Shank to promote spine head enlargement.

If Shank binding to endogenous Homer is important for spine head expansion, then it might be expected that mutants (1-1440) and (P1497L) would have dominant-negative effects on spine growth, since they should interfere with recruitment of endogenous Homer. Detailed morphometric analysis showed a tendency of Shank1B(P1497L) and Shank1(1-1440) to reduce spine head width in transfected neurons, but the difference in means did not reach statistical significance (Table 1; Figures 4C and 4D). Rather, the most striking and statistically significant effect of the (1-1440) and (P1497L) mutants was to reduce the linear density of dendritic spines in transfected neurons by ~50% (Figure 4B; number of spines per 10 μm dendrite length = 1.6 ± 0.4 [(1-1440)] and 1.8 ± 0.4 [(P1497L)], compared with 3.2 ± 0.2 [GFP + Shank1B] or 3.3 ± 0.3 [GFP alone]; $p < 0.01$). We undertook an additional dominant-interfering approach by overexpressing Shank1(481-840), the smallest Shank construct tested that shows robust synaptic targeting (Figure 3A). Shank1(481-840) would be expected to compete for synaptic recruitment of endogenous Shank (which is dependent on its PDZ interaction with the C terminus of GKAP). Interestingly, the primary effect of Shank(481-840) on spines was also a reduction in spine number (Figure 4B; 1.5 ± 0.2 spines per 10 μm dendrite versus 3.3 ± 0.2 GFP control; $p < 0.01$). In the case of Shank1(481-840), however, there was also a statistically significant reduction in spine length (0.98 ± 0.26 μm from 1.28 ± 0.5 μm; $p < 0.05$) and width (0.53 ± 0.14 μm from 0.68 ± 0.25 μm; $p < 0.05$) (Figures 4Ae1, 4C, and 4D; Table1). We could not directly assay for loss of endogenous Shank from synapses, using dominant-negative construct Shank1(481-840), since our Shank antibodies would also react with the transfected construct. However, the depletion of endogenous synaptic Homer (see below) strongly suggests that Shank1(481-840) displaced endogenous Shank from synapses.

In addition to the Homer binding motif, a postsynaptic localization was also needed for Shank to exert its effect on dendritic spines. The Shank1B(ΔSP) mutant lacking SH3 and PDZ domains had no influence on the size of spines, even though it contained the Homer binding site (Figures 4Af1, 4C, and 4D). Taken together, our data indicate that Homer binding is required for the spine-promoting activity of Shank and that the Shank protein needs to be concentrated at postsynaptic sites for the effect.

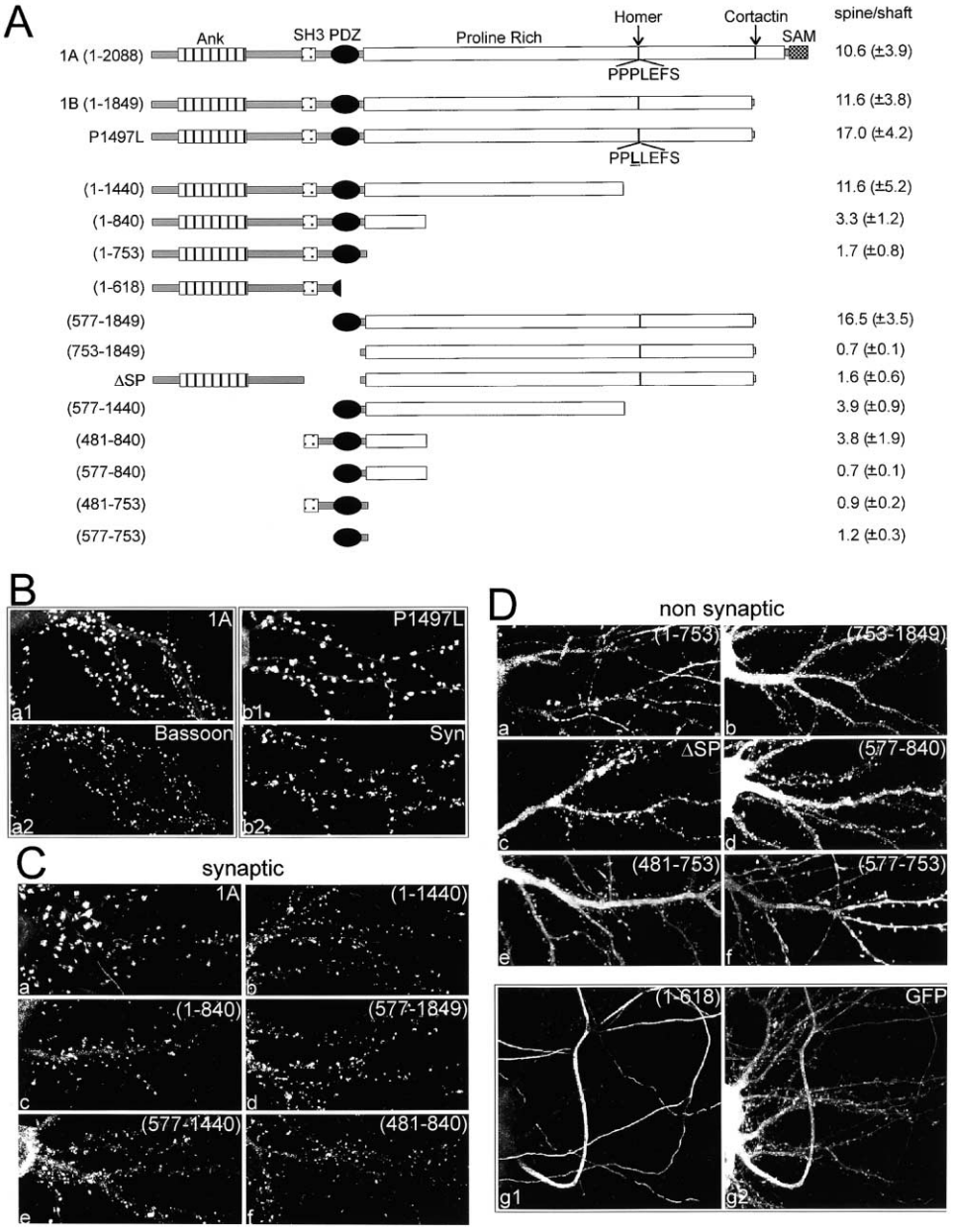

Figure 3. Determinants of Synaptic Targeting of Shank1

(A) Diagram of wild-type and mutant constructs of Shank1 (all HA-tagged at the N terminus) used in this study. The various domains, Homer binding motif, and cortactin binding site are indicated. Ank, ankyrin repeats. Synaptic targeting of each construct is quantified to the right by the ratio of staining intensity in spine/shaft (at least four neurons examined for each construct).

(B) Neurons were transfected with Shank1A (Ba1 and Ba2) or Shank1B(P1497L) (Bb1 and Bb2) at DIV14 and double-stained at DIV18 with antibodies to HA (Ba1 and Bb1) and Bassoon (Ba2) or synaptophysin (Bb2). Wild-type Shank1A and Shank1B(P1497L) mutant colocalized with both presynaptic markers.

(C and D) Neurons transfected with wild-type Shank1A or mutant Shank constructs (as indicated in each panel) were stained with HA antibodies to visualize the transfected Shank protein (as in [Ba1] and [Ba2]). (C) Examples of Shank constructs that showed specific localization in synapses (colocalization with presynaptic markers not shown). (D) Examples of Shank mutants that failed to localize specifically in synapses. For the (1-618) construct, which fills the axon (Dg1), cotransfected GFP is also shown to visualize the cell body and dendrites (Dg2).

Homer and Shank Cooperate in Promoting Spine Growth

Shank requires Homer binding for its effect on spines; however, overexpression of Homer1b (a splice variant of Homer1, containing the coiled-coil multimerization domain) in the absence of Shank had no significant effect on spine dimensions (Figures 5A, 5C, and 5D; Table1). The lack of effect may be due to the fact that exogenous Homer1b was diffusely expressed in neurons (Figure 5Ab2), unlike endogenous Homer, which is selectively enriched in synapses (see Figure 6). Reasoning that Homer may depend on Shank for localization

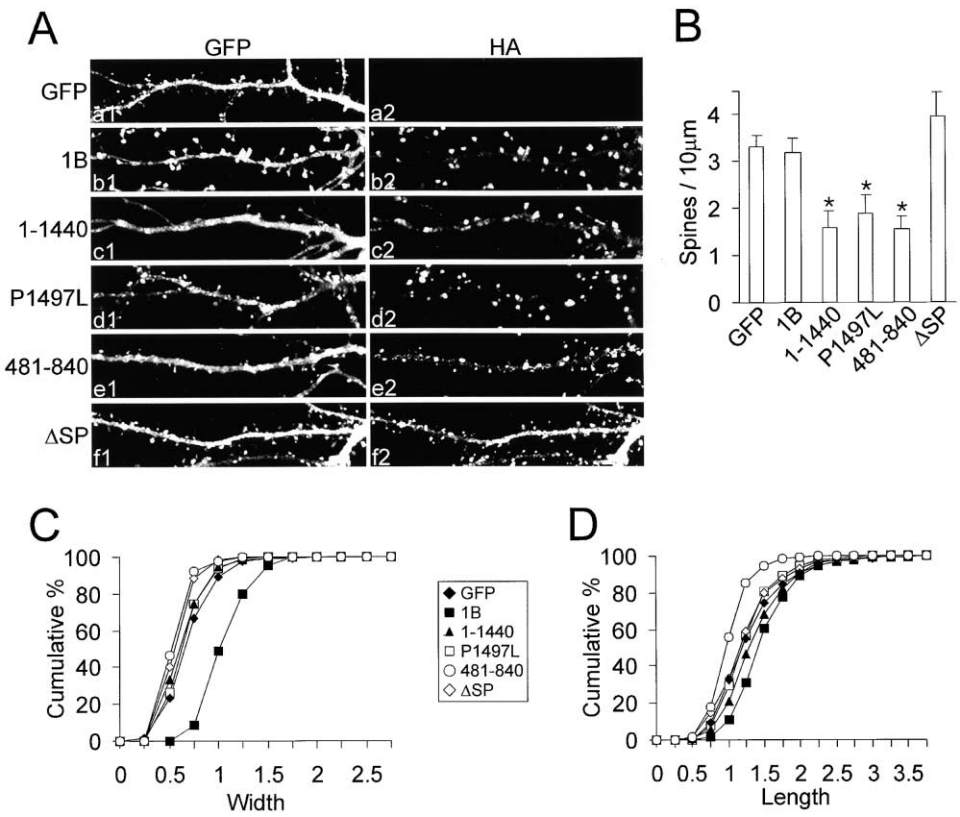

Figure 4. Homer Binding Site and Synaptic Localization Required for Spine Enlargement by Shank

Neurons were transfected at DIV12 and examined at DIV18. (A) Neurons were transfected with GFP + Shank constructs as indicated to the left. Each pair of images ([Aa1] and [Aa2], etc.) shows double labeling for exogenous Shank protein by HA antibodies (right) and for GFP to assess spine morphology (left). The first row (Aa1 and Aa2) was transfected with GFP alone. 1B, Shank1B. (B) Quantitation of spine density (number of spines per 10 μm dendrite length) in neurons transfected as in (A) (at least eight neurons examined for each construct). Histogram shows mean ± SD. *, $p < 0.01$.

(C and D) Cumulative frequency plots showing distribution of spine head width (μm) and spine length (μm) in neurons transfected as in (A) (>600 spines and >8 neurons examined for each construct).

in synapses, we cotransfected neurons with Homer1b and Shank1B (and GFP). In these neurons, exogenous Homer was specifically targeted to dendritic spines, colocalizing closely with exogenous Shank1B (Figures 5Ba1–5Ba3). In neurons overexpressing both Homer1b and Shank1B, spine heads exhibited dramatic enlargement, surpassing even that of Shank1B-transfected neurons (Figures 5Ba1, 5C, and 5D; Table 1). The length of spines also increased with Shank1B/Homer1b coexpression (Figure 5D), but this was largely attributable to expansion of the spine head.

Homer1b failed to accumulate in dendritic spines when cotransfected with the Shank1(1-1440) or Shank1B(P1497L) mutants that lack the Homer binding site (Figures 5Bb1–5Bb3 and data not shown). In these cotransfected neurons, exogenous Homer was diffusely distributed in the cytoplasm of dendrites and soma (Figure 5Bb3), even though the Shank mutant was localized in dendritic spines (Figure 5Bb2). Significantly, the neurons coexpressing Homer1b and Shank1(1-1440) did not show enlarged spines (Figure 5Bb1). Thus, the synaptic accumulation of Homer depends on its interaction with Shank and correlates with the ability of Shank/Homer to induce enlargement of spine heads.

Spine enlargement by Shank1B or Shank1B + Homer1b was not prevented by culturing transfected neurons in the presence of blockers of NMDA receptors (APV, 100 μm), AMPA receptors (CNQX, 100 μm), and mGluRs (4-CPG + AIDA, 500 μm) from the time of transfection (data not shown). These results argue that the effect of Shank/Homer on spine size is not activity dependent.

Shank Recruits Endogenous Homer to Synapses

The above experiments indicate that exogenous Shank1 can recruit exogenous Homer1b to synapses. Does transfected Shank also recruit endogenous Homer proteins to mediate its effect on dendritic spines? In neurons transfected with Shank1B alone (Figure 6A, left), there was an increase in immunofluorescence staining intensity for endogenous Homer at synapses (2.9 ± 0.2 relative to control; $p < 0.01$), colocalizing with the exogenous Shank protein. In contrast, neurons transfected with Shank1(1-1440), which lacks the Homer binding site, showed a markedly reduced level of endogenous Homer (Figure 6A, right; 0.2 ± 0.09 relative to control; $p < 0.01$). Transfection of mutant P1497L also decreased the staining of endogenous Homer at synapses

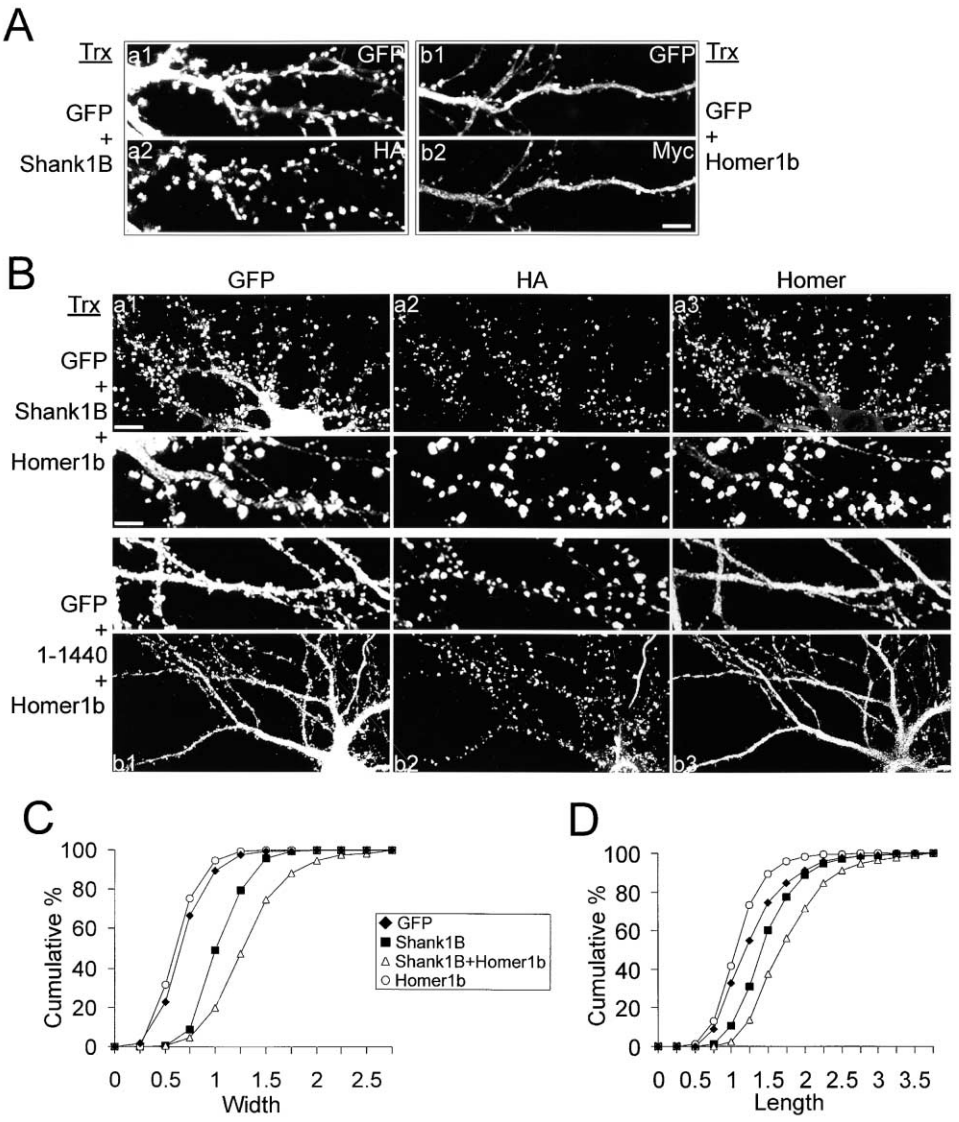

Figure 5. Homer and Shank Cooperate to Promote Spine Enlargement

(A) Neurons transfected with Shank1B and GFP (left) compared with neurons transfected with Homer1b and GFP (right). Pairs of images ([Aa1]/[Aa2] and [Ab1]/[Ab2]) show double labeling for GFP and exogenous proteins as indicated (HA antibodies for Shank1B, and Myc antibodies for Homer1b).

(B) Neurons were triply transfected with GFP, Homer1b, and Shank1B wild-type or (1-1440). Each triplet of images ([Ba1]/[Ba2]/[Ba3], etc.) shows triple labeling for GFP (to visualize dendritic spine morphology), exogenous Shank (HA antibodies), and exogenous Homer1b (Homer antibodies). Insets show higher magnification views. Scale bar: 10 μm for main panels, 5 μm for insets.

(C and D) Cumulative frequency plots of spine head width and spine length (in μm) in neurons transfected as described in (A) and (B) (>600 spines and >8 neurons examined for each condition).

(Figure 6B). In triple-label experiments, exogenous Shank1B(P1497L) (red) accumulated in bright puncta that colocalized with synaptophysin staining (blue) (magenta in merge), confirming the synaptic localization of this Shank mutant (Figure 6B, arrows). These same synapses that contained Shank1B(P1497L) also showed diminished staining for endogenous Homer (0.3 ± 0.15 relative to control, $p < 0.01$; Figure 6B), resulting in lack of white (blue, red, and green) puncta in the merged picture. As "internal control," nearby dendrites from cells not transfected with Shank1B(P1497L) showed obvious punctate labeling for endogenous Homer that colocalized with synaptophysin (cyan in merge) (Figure 6B, arrowheads). Thus, not only is Shank1B(P1497L) incapable of recruiting endogenous Homer to synapses, it actually inhibits the normal synaptic accumulation of Homer. As expected, overexpression of Shank1(481-840) also reduced the synaptic staining of endogenous Homer, while Shank1BΔSP, which is not targeted to synapses, had no effect (data not shown). Taken together, these data demonstrate that synaptically targeted Shank can recruit endogenous Homer to dendritic spines. Moreover, Shank mutants defective in Homer binding act as interfering constructs to deplete endoge-

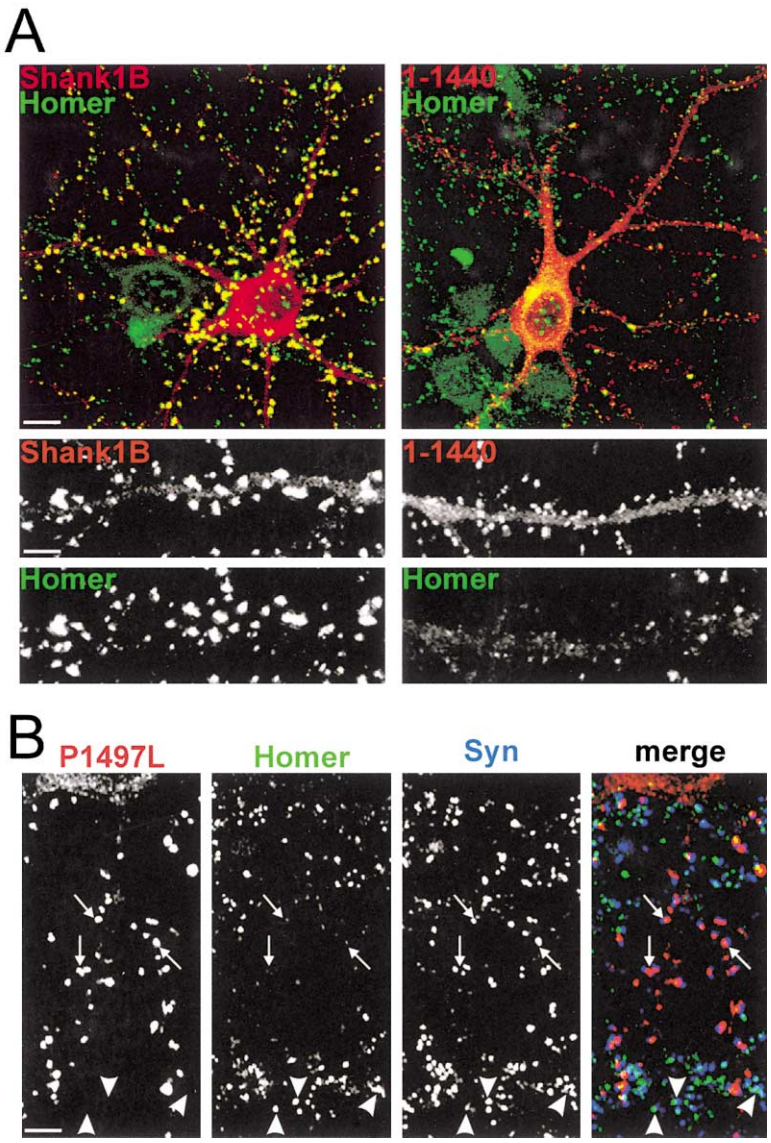

Figure 6. Shank Recruits Endogenous Homer to Synapses

(A) Neurons were transfected with wild-type Shank1B (left) or Shank1(1-1440) (right) and double stained for endogenous Homer (green) and for exogenous Shank (red). Note untransfected cells in both panels with green punctate staining of Homer. Lower panels show, at higher magnification and in grayscale, the individual Shank and Homer channels. Shank1B overexpression recruits endogenous Homer to spines, whereas Shank1(1-1440) reduces endogenous Homer in spines. (B) Neurons were transfected with Shank1B(P1497L) and triple labeled for exogenous Shank (red), endogenous Homer (green), and endogenous synaptophysin (blue). Individual channels are shown in grayscale for better resolution and more quantitative representation of staining intensity. Dendritic spines containing the Shank1B(P1497L) Shank mutant (arrows) overlap closely with synaptophysin but show a decrease in staining of endogenous Homer, resulting in magenta puncta in merge (arrows). In dendritic spines lacking Shank1B(P1497L), there is punctate enrichment of endogenous Homer (arrowheads) that colocalizes with synaptophysin, resulting in cyan puncta in merge (arrowheads).

nous Homer from synapses, correlating with their ability to reduce spine number and/or size.

Effect of Shank and Homer on Other Synaptic Proteins

We examined the effect of Shank overexpression on synaptic levels of GKAP and PSD-95 in triple-labeling experiments (Figure 7A). In neurons transfected with Shank1B or Shank1B + Homer1b, the exogenous Shank protein colocalized with endogenous GKAP and PSD-95 in the enlarged dendritic spines (white in merge, Figure 7A), again confirming the postsynaptic targeting of transfected Shank. The intensity of GKAP staining in dendritic spines was increased slightly in Shank1B-transfected neurons (1.3 $\pm$ 0.18 relative to control, $p < 0.05$) and greatly in neurons cotransfected with Shank1B + Homer1b (2.6 $\pm$ 1.3, $p < 0.01$; Figure 7A; quantitation in Figure 8E). The staining intensity of PSD-95 also increased in spines of neurons overexpressing Shank1B or Shank1B/Homer1b, but the effect was more modest than that seen with GKAP (1.2 $\pm$ 0.37, $p = 0.18$; and 1.7 $\pm$ 0.46, $p < 0.05$, respectively; Figures 7A and Figure 8E). There was no increase in postsynaptic staining of GKAP or PSD-95 in neurons transfected with Shank1B(P1497L) or (1-1440), mutants that do not bind Homer and that do not promote spine enlargement (Figures 7A and 8E). Thus, there was a correlation between spine head enlargement induced by Shank/Homer and the staining intensity of PSD-95 and GKAP in those spines. These results are consistent with an expansion of the PSD in the Shank/Homer-enlarged spine heads. Interestingly, we observed that a large proportion of spines in neurons overexpressing Shank1B (45.2% $\pm$ 4.5%) and Shank1B + Homer1b (67.7% $\pm$ 1.9%) contained multiple discrete clusters of PSD-95 (Figure 7A, arrowheads), compared with only 6.1% $\pm$ 1.2% in untransfected neurons. These findings are suggestive of split PSDs in the enlarged spine heads of Shank-transfected neurons. However, ultrastructural analysis is needed to confirm this possibility.

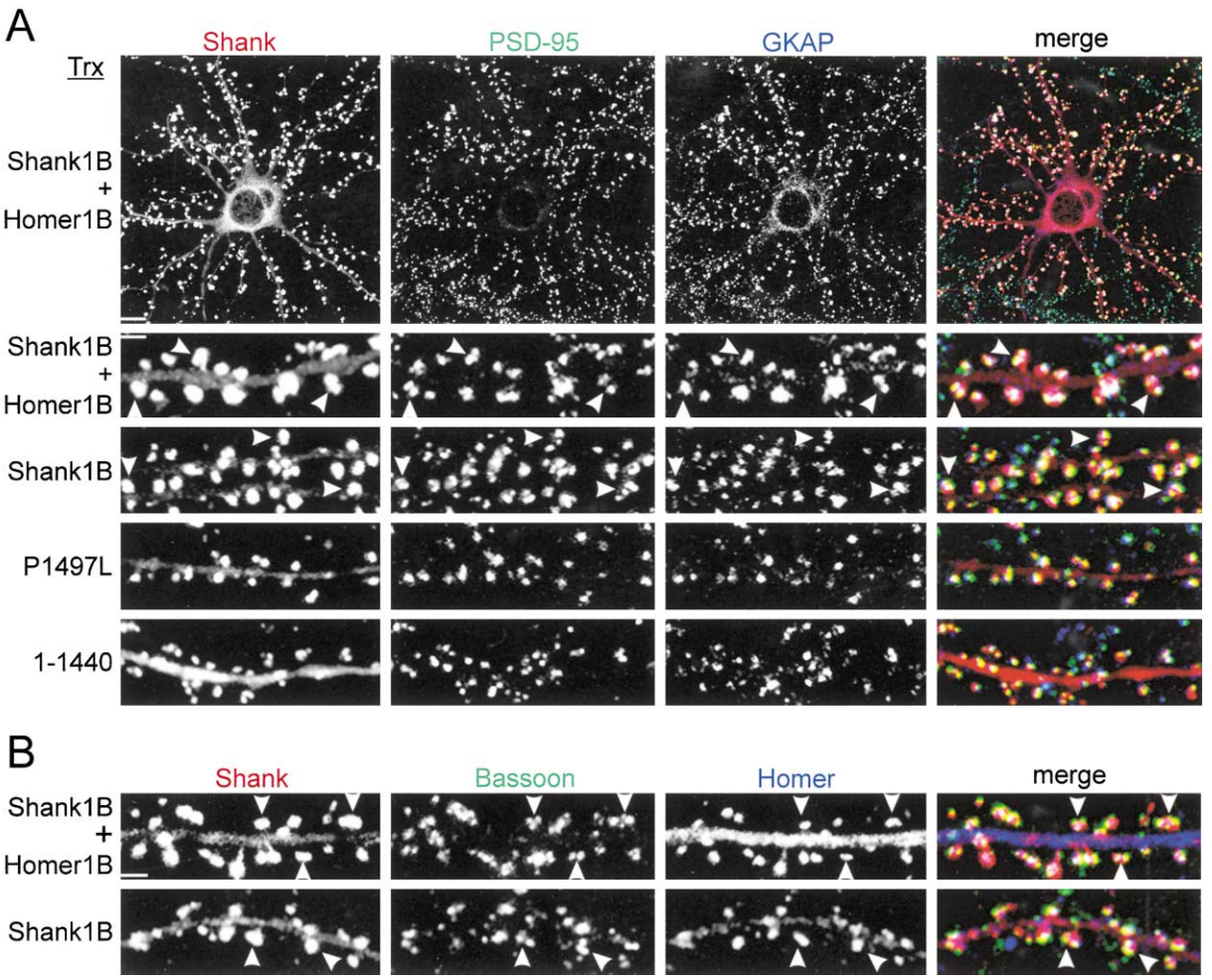

Figure 7. Effect of Shank and Homer on PSD-95, GKAP, and Bassoon

(A) Neurons were transfected with Shank1B or Shank1 mutants (P1497L) or (1-1440), with or without Homer1b, as indicated to the left. Each row of images shows triple labeling for Shank (red), PSD-95 (green), and GKAP (blue). Far right panel shows merge in color. Individual channels are shown in grayscale for better resolution and more quantitative representation of staining intensity. Scale bar: 10 μm for top row (low magnification), 2.5 μm for other rows. Arrowheads indicate examples of enlarged spines in Shank1B- or Shank1B/Homer1b-transfected neurons that show multiple distinct clusters of PSD-95.

(B) Neurons were transfected as indicated to the left and triple labeled for Shank (red), Bassoon (green), and Homer (blue). Arrowheads indicate examples of enlarged spines in Shank1B- or Shank1B/Homer1b-transfected neurons that are associated with multiple distinct clusters of Bassoon. Scale bar, 2.5 μm.

In triple-labeling studies of neurons transfected with Shank1B or with Shank1B + Homer1b, most if not all of the spines labeled for exogenous Shank protein have a presynaptic contact, as defined by punctate colocalization with Bassoon (Figure 7B) or synaptophysin (data not shown). Indeed, the staining intensity for Bassoon associated with Shank- or Shank/Homer-transfected neurons was slightly increased (Figure 8E). To a similar extent as with PSD-95, Bassoon and synaptophysin staining was frequently split into multiple distinct clusters associated with individual enlarged spines in neurons overexpressing Shank1B or Shank1B + Homer1b (Figure 7B, arrowheads; data not shown).

Shank and Homer Recruit IP3 Receptor and F-Actin to Spines

Homer binds directly to the IP3 receptor, which is localized in the SER. In brain, SER is found particularly in large dendritic spines (Spacek and Harris, 1997). We therefore investigated the possibility that Shank and Homer may recruit IP3 receptor (and by inference SER) to spines. In untransfected or vector-transfected hippocampal neurons, IP3 receptor immunoreactivity was not concentrated at synaptic sites, though a diffuse somatodendritic and axonal staining was observed (Figure 8A). In neurons transfected with Shank1B, however, IP3 receptors became enriched in the majority of spines (Figure 8A; 2-fold increase in staining intensity, quantified in Figure 8E). The recruitment of IP3 receptors to spines by Shank may be mediated by Homer. Indeed, neurons cotransfected with Shank1B + Homer1b showed a further increase (5-fold relative to control) of IP3 receptor staining in spines (Figures 8A and 8E). Enhanced IP3 receptor staining in dendritic spines was not seen in neurons transfected with the Shank1(1-1440) mutant (Figures 8A and 8E) or the Shank1B(P1497L) mutant

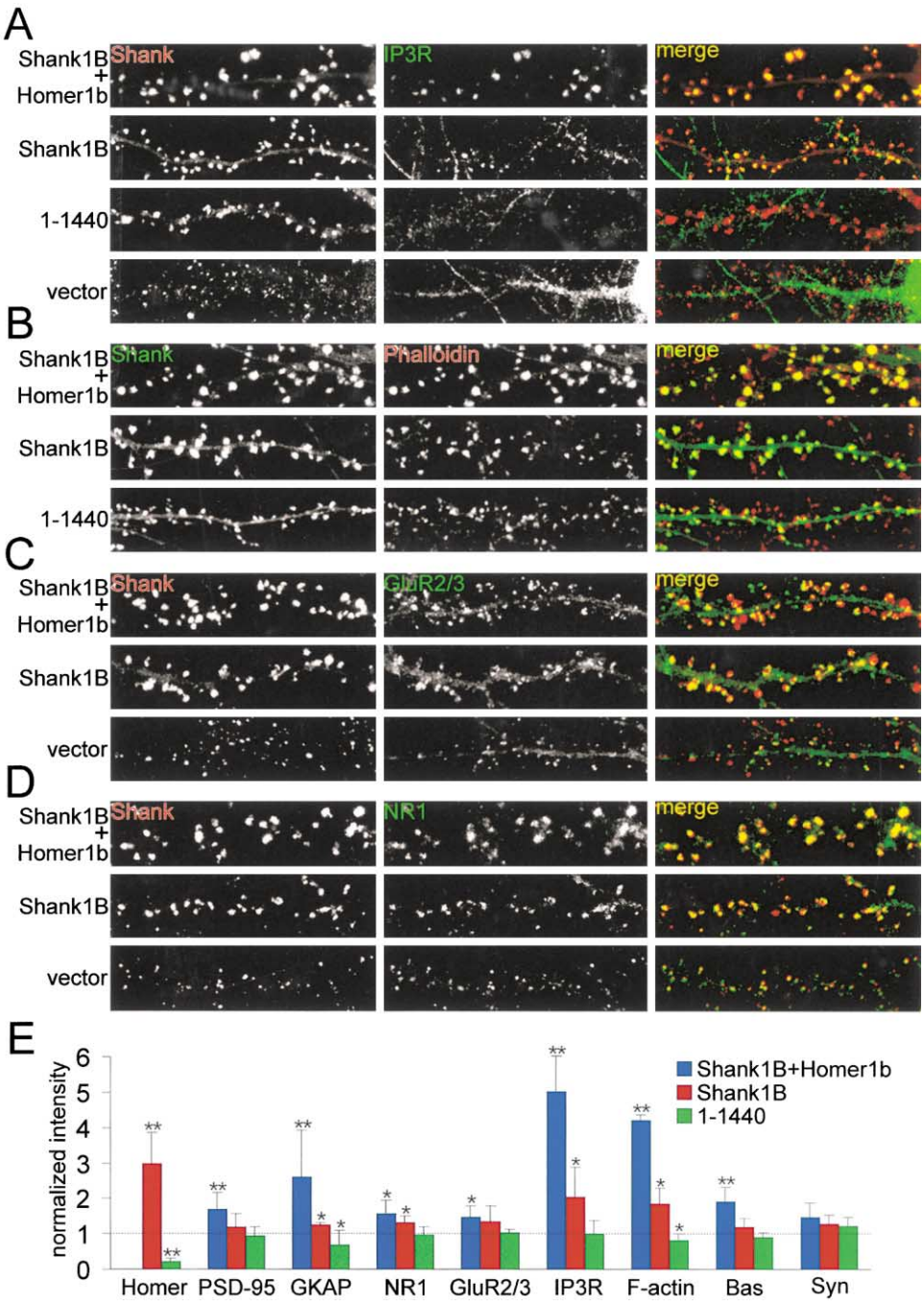

Figure 8. Shank and Homer Recruit IP3 Receptor and Other Postsynaptic Proteins

(A) Neurons were transfected with Shank constructs ± Homer1b as indicated to the left. Each row shows double labeling for Shank (red, left panel) and IP3 receptor (green, middle panel); merge is shown in the right panel. Individual channels are shown in grayscale.

(B) Neurons transfected as in (A) were double labeled for Shank (green) and F-actin (phalloidin; red).

(C and D) Neurons transfected as in (A) were double labeled for Shank (red) and for GluR2/3 (C) and NR1 (D) (green). Scale bar, 5 μm.

(E) Quantitation of changes in synaptic staining intensity of the indicated proteins induced by overexpression of Shank1B + Homer1b, Shank1B, or Shank1 (1-1440). At least six neurons were analyzed for each endogenous protein; 30 to 50 synapses were scored per neuron. Histograms show mean ± SD normalized to the staining intensity in untransfected neurons. *, $p < 0.05$; **, $p < 0.01$.

(data not shown), both of which lack the Homer binding site. These data demonstrate that Shank, via its ability to bind and recruit Homer, can increase the abundance of IP3 receptor in dendritic spines.

We also observed an increase in F-actin content (measured by phalloidin staining) in spines of Shank-transfected neurons and a further increase in neurons cotransfected with Shank and Homer (Figures 8B and 8E). Phalloidin staining in neurons transfected with Shank1(1-1440) mutant was similar to control. Thus, en-

largement of dendritic spines by Shank and Homer is correlated with buildup of F-actin in these spines. The recruitment of IP3 receptor and F-actin imply that, in addition to physical enlargement of the spine head, Shank/Homer also govern the cytoskeletal and intracellular membrane contents of dendritic spines.

Finally, we examined the staining of endogenous glutamate receptors. In neurons overexpressing Shank1B, there was a slight but significant increase in synaptic staining of NMDA receptor subunit NR1 (1.4 ± 0.18 relative to control, $p < 0.05$) in Shank-transfected neurons and a significant increase of both NR1 (1.6 ± 0.39, $p < 0.05$) and AMPA receptor subunits GluR2/3 (1.5 ± 0.30, $p < 0.05$) in neurons cotransfected with Shank1B + Homer1b (Figures 8C–8E). In general, the largest effects of Shank/Homer on synaptic protein levels were on those molecules that interact most directly with Shank or Homer, namely, GKAP, Homer, and IP3 receptor.

Effects of Shank on Synaptic Function

Given the structural and molecular changes induced by Shank overexpression, we explored functional synaptic effects by measuring the peak amplitude and frequency of miniature excitatory postsynaptic currents (mEPSCs) in transfected neurons. The physiological effects of Shank overexpression were tested in both DIV17 and DIV11 neurons (transfected at DIV5–6), since recent findings indicate that neurons younger than DIV14 tend to exhibit an "immature" type of synaptic transmission that lacks AMPA receptor-mediated responses, while neurons after DIV14 show a "mature" functionality incorporating the AMPA-mediated component (Renger et al., 2001). In immature neurons (DIV11), transfection of GFP + Shank had little effect on mEPSC amplitude but markedly increased mEPSC frequency compared with GFP-only neurons (Figures 9A and 9C; $n = 15$ for GFP + Shank, 9 for GFP control; $p < 0.05$). In mature (DIV17) neurons, Shank transfection resulted in a small but surprising decrease in mEPSC amplitude (Figures 9A and 9C; $n = 9$ for GFP + Shank, 9 for GFP control; $p < 0.05$), while minifrequency was modestly increased.

Since changes in mEPSC frequency generally reflect presynaptic effects, we used FM4-64 dye uptake to evaluate the number and functional vesicle pool size of presynaptic terminals contacting transfected neurons. Indeed, Shank overexpression was associated with a marked increase in FM4-64 staining density that correlated with the elevated minifrequency in both immature and mature neurons (Figures 9B and 9C). Thus, both FM4-64 imaging and electrophysiological data indicate that enhancement of presynaptic function is a major outcome of postsynaptic Shank overexpression.

Discussion

Regulation of Spine Size and Number by Shank

We have shown here that overexpression of a single protein, Shank, can promote the maturation and growth of dendritic spines—the morphological effect being primarily an enlargement of the spine head. In developing brain, Shank expression increases in parallel with synaptogenesis (Boeckers et al., 1999a; Lim et al., 1999). At early ages in culture (DIV7), when endogenous Shank is expressed at low levels in neurons (C.S., unpublished data), spines are poorly developed and have a filopodial appearance. Expression of Shank during the first week in culture accelerates the development of mushroom spines, at the expense of filopodia-like extensions. Even at 2 weeks in vitro, when endogenous expression of Shank has increased and neurons have developed many mushroom-like spines, Shank overexpression is still capable of stimulating the enlargement of most if not all spine heads in the transfected neuron. These findings imply that the level of endogenous Shank protein in neurons is limiting for maturation and growth of the spine head. On the other hand, normal endogenous Shank levels seem not to be the limiting factor for the formation of spines, at least from DIV5 onward, since Shank overexpression at this stage and later does not lead to increased spine numbers.

Although the dominant-negative Shank mutants [(1-1440), (P1497L), and (481-840)] tend to cause a reduction in spine size, it is notable that their major effect was an ~50% reduction in spine density (Figure 4; Table 1). This contrasts with Shank overexpression, which predominantly affects spine size rather than numbers. There are several reasonable explanations for this apparent discrepancy. First, normal spines may need to mature and grow to a certain size before they become "stable." Dominant-negative Shank constructs would interfere with the normal maturation and growth of spines (perhaps arresting them in a filopodia-like stage), leading to a higher proportion of unstable spines that eventually disappear. This would be manifested ultimately as reduced spine density. We favor this explanation, since dendritic spines are believed to be highly plastic/motile structures that develop through relatively unstable intermediates (Harris, 1999a). According to this hypothesis and consistent with the dominant-negative data, physiological levels of Shank are required to promote the maturation, growth, and stability of dendritic spines.

An alternative explanation (not mutually exclusive) is that dominant-negative Shank and the consequent depletion of synaptic Homer cause the shrinkage of a subset of spines, such that many fall below the limit of detection in our "GFP-fill" confocal microscopy measurements. (This reduction in spine density would be analogous to the apparent reduction in mEPSC frequency seen when there is a decrease of EPSC amplitudes that are close to "noise" levels.) Finally, it is possible that Shank is a relatively direct determinant of spine numbers (i.e., Shank is important for initiating the formation of spines), and the dominant-negative constructs reduce Shank activity below the critical level for promoting spine formation. However, a direct instructive role for Shank in spinogenesis is not supported by the lack of effect of Shank overexpression on spine density and the abundant synaptic presence of Shank in nonspiny neurons (C.S. and M.S., unpublished data).

Role of Homer in Spine Morphogenesis

Synaptic recruitment of Homer appears to be a critical factor in Shank's ability to induce bigger spines: Homer binding is critical for the spine-promoting activity of Shank, and there is a correlation between synaptic Homer levels and spine size. How might Homer be in-

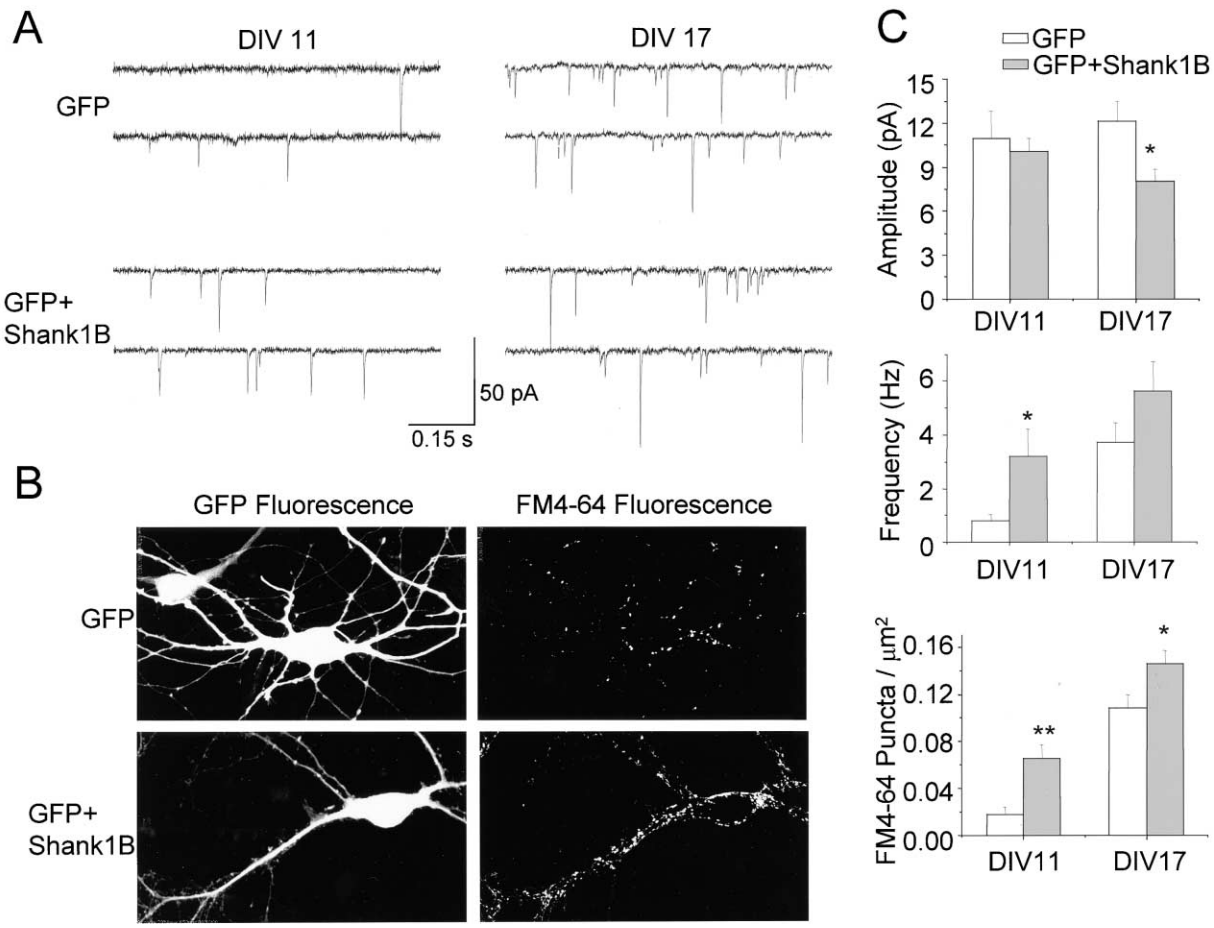

Figure 9. Functional Synaptic Effects of Shank Overexpression

Neurons transfected with GFP and Shank1B were compared with control neurons transfected with GFP only. (A) Example recordings of AMPA receptor-mediated mEPSCs from neurons at DIV11 and DIV17. (B) FM4-64 staining of functional presynaptic terminals on transfected neurons at DIV11 (transfected cell outline shown by GFP fluorescence). (C) Quantitation of mEPSC peak amplitude (top), mEPSC frequency (middle), and puncta density of FM4-64 staining (bottom; see Experimental Procedures) in cells at DIV11 and DIV17. Histograms show mean plus SEM. *, $p < 0.05$; **, $p < 0.01$

volved in the enlargement of spine heads? The Homer family of proteins binds to the PPXXF motif found in Group I mGluRs, IP3 receptors, ryanodine receptors, and Shank—these interactions being mediated by the N terminally located EVH1 domain of Homer (Tu et al., 1998, 1999). By physically linking mGluR1α and mGluR5 with ER-associated IP3 receptors, multimeric Homer is believed to aid the coupling of these surface receptors to intracellular calcium release (Tu et al., 1998; Xiao et al., 1998). Our study shows that Shank recruits IP3 receptors (and by inference SER) to dendritic spines in a Homer-dependent manner. Since calcium release from intracellular stores has been implicated in the regulation of spine morphology (Harris, 1999b; Korkotian and Segal, 1999), Homer could promote spine enlargement by enhancing intracellular calcium responses to activation of mGluRs or other postsynaptic receptors.

In addition, the C-terminal region of Homer (more specifically Cupidin/Homer2a) has been shown to bind in vitro to Rho family GTPases such as Rac1 (Shiraishi et al., 1999), which is implicated in regulation of dendritic spines (Nakayama et al., 2000). Thus, Homer may have actin regulatory properties that underlie its ability to promote spine enlargement, perhaps as an effector or modulator of Rho-family GTPases. However, arguing against a major role for Rac in the Shank/Homer effect is that Shank and Homer do not have the same morphological effects as activation of Rac, which results in disruption of normal spine morphology and formation of ruffles and long filopodia-like processes (Nakayama et al., 2000). In contrast, the altered spines induced by Shank overexpression show a relatively smooth enlargement of the spine head and little change in spine length or number.

Role of Shank in Postsynaptic Molecular Organization and Presynaptic Function

Not only does Shank increase the dimensions of the spine head, it also alters the molecular and organelle content of the dendritic spine. In Shank-enlarged spines, there was accumulation of IP3 receptors, as well as Homer, GKAP, F-actin, and, to a lesser extent, PSD-95, NR1, and GluR2/3. The increased levels of these postsynaptic proteins suggest an expansion of the syn-

apse that accompanies growth of the spine head. Interestingly, however, electrophysiological measurements and FM4-64 staining suggests that the major functional effect of postsynaptic Shank overexpression is one of presynaptic, rather than postsynaptic, enhancement. In this sense, the results are reminiscent of a recent study (El-Husseini et al., 2000) in which PSD-95 overexpression in developing neurons caused spine enlargement that was accompanied by a 10-fold increase in mEPSC frequency but only a 30% increase in mEPSC amplitude. In both these cases, a retrograde signal must be invoked to transmit the effects of postsynaptic expression of PSD-95 and Shank to enhancement of presynaptic neurotransmitter release.

Nevertheless, there is an interesting difference between the electrophysiological effects of overexpressing Shank (this study) and PSD-95 (El-Husseini et al., 2000). Shank overexpression did not increase mEPSC amplitude in young neurons and was even associated with a reduced mEPSC amplitude in mature neurons. How can this be reconciled with Shank-induced enlargement of spines and increased staining of various postsynaptic proteins? A possible explanation comes from the morphological evidence for multisynapse spines in Shank-transfected neurons, in which individual enlarged spine heads were associated with multiple discrete clusters of PSD-95 and Bassoon. This putative "synapse splitting" was observed in a large proportion of spines in Shank- and Shank/Homer-transfected neurons (40%–50% and 60%–70%, respectively) but relatively rarely in control neurons (5%–7%). Ultrastructural studies are required to confirm that the multiple puncta of PSD-95 or Bassoon staining actually represent multisynapse spines; however, synapse splitting of this sort could explain why mEPSC amplitudes are unchanged or decreased despite overall accumulation of postsynaptic proteins in individual enlarged spines. Since spine growth and synapse splitting has been correlated with long-term synaptic potentiation (Engert and Bonhoeffer, 1999; Maletic-Savatic et al., 1999; Toni et al., 1999), our findings raise the possibility that Shank may be involved in the molecular mechanisms underlying such forms of activity-dependent structural plasticity.

Since the postsynaptic level of Shank protein appears limiting for Homer recruitment and spine enlargement, one might speculate that increasing the endogenous expression of Shank could stimulate the growth of spines. Interestingly, Shank1 mRNA is localized in dendrites (Zitzer et al., 1999a; M.P. and M.S., unpublished data), potentially allowing postsynaptic translation of Shank (Steward and Schuman, 2001) and hence local control of spine morphology by Shank. Another possibility is that the activity of Shank in the PSD might be controlled by posttranslational modification—for instance, phosphorylation could regulate Shank-Homer protein-protein interaction. It will be interesting therefore to determine whether the expression, subcellular distribution, and/or phosphorylation state of Shank is controlled by neural activity and how these changes contribute to the functional and structural plasticity of synapses.

Experimental Procedures

Neuron Culture

Hippocampal neuron cultures were prepared from E18-E19 rat hippocampi. High-density (750–1000 cells/mm^2) neurons were plated and grown as described in (Sala et al., 2000). Medium-density neurons (150–200 cells/mm^2) were prepared (as described in Brewer et al., 1993). Neurons were transfected using calcium phosphate precipitation, and the transfection efficiency was ~1%.

Recombinant DNA

Full-length Shank1A and Shank1B cDNAs (described in Lim et al., 1999; Naisbitt et al., 1999) were used as templates for all the constructs shown in Figure 3A. N-terminal HA-tagged versions of Shank1A and Shank1B, deletion, and point mutant constructs were made as follows. A fragment from amino acid 1 to amino acid 618 of Shank1A was amplified by PCR, digested with AscI-EcoRI, and subcloned in-frame into a GW1-CMV expression vector (British Biotechnology) with a built-in N-terminal HA tag (N-HA-GW1 vector). This cDNA represents the deletion mutant (1-618). For full-length Shank1A, Shank1B, and constructs (1-1440) and (1-840), an EcoRI-EcoRI fragment containing the second part of the protein was then subcloned into the (1-618) plasmid. Deletion mutant (753-1849) was made by subcloning a BglII-EcoR1 fragment into the N-HA-GW1 vector. For the (557-1849) and the ΔSP deletions, respectively, an AscI-BglII fragment from 557 to 752 and from 1 to 480 was subcloned into the (753-1849) construct. The point mutant (P1497L) was made using the QuikChange system (Stratagene). The other deletion constructs were made by PCR amplification using appropriate oligos and Shank1B cDNA as template. All constructs were checked by sequencing and by expression of proteins of the expected molecular weight in COS-7 cells. Myc-tagged Homer1b was provided by Paul Worley (Xiao et al., 1998).

Immunostaining and Antibodies

After transfection (3–6 days), neurons were fixed in 4% paraformaldehyde and 4% sucrose at room temperature or in 100% methanol at −20°C for 10 min. Primary and secondary antibodies were applied in GDB buffer (30 mM phosphate buffer [pH7.4] containing 0.2% gelatin, 0.5% Triton X-100, and 0.8 M NaCl). The following antibodies/probes were used (source of antibody in parentheses): mouse anti-GFP antibodies (Quantum); rat and mouse monoclonal anti-HA antibodies (Boehringer); mouse monoclonal anti-Myc epitope (Santa Cruz Biotechnology); Shank antibodies Shank 56/e (Naisbitt et al., 1999); GKAP rabbit N1546 (Kim et al., 1997); PSD-95 mouse monoclonal K28/43.1 (gift from J. Trimmer); Shank guinea pig #1123, Homer rabbit 1133 (gift from E. Kim, Korean Advanced Institute of Science and Technology [KAIST], Taejon, Korea); IP3 receptor rabbit (PA3-901; Affinity Bioreagents Inc.); Bassoon mouse monoclonal 7F407.3 (gift from C. Garner, University of Alabama); synaptophysin mouse monoclonal (Sigma); NR1 mouse monoclonal (PharMingen); GluR2/3 rabbit (Chemicon); FITC-, Cy3-, and Cy5-conjugated secondary antibodies (Jackson ImmunoResearch Labs); Texas red-conjugated phalloidin (Molecular Probes). Fluorescence images were acquired using Biorad MRC1024 confocal microscope.

Image Acquisition and Quantification

Confocal images were obtained using a Zeiss 63× objective with sequential acquisition setting at 1280 × 1024 pixels resolution. Each image was a z series projection of approximately 7 to 15 images, each averaged two to three times and taken at 0.5–1 μm depth intervals. Labeled transfected neurons were chosen randomly for quantification from two to five coverslips from two to six independent experiments for each construct. The number of neurons used for quantification is indicated in the figure legends. Morphometric measurements were performed using MetaMorph image analysis software (Universal Imaging Corporation). Single dendrites were selected randomly, and each individual spine present on the dendrites was manually traced (examples shown in Figure 2E). The maximum length and head width of each spine was automatically measured by computer and logged into Microsoft Excel. The ratio of average immunofluorescence intensity between the spine head and the dendritic shaft was measured on manually selected spine head and dendritic shaft areas.

Fluorescence intensity of staining of endogenous protein was measured as mean intensity of synaptic areas in transfected and untransfected neurons. Synaptic areas were defined by staining for Shank in one fluorescence channel. The ratio was obtained by comparing values in transfected cells versus untransfected cells.

The 3D graphs of spine length and width distributions (Figure 2) were constructed by sorting the length and the corresponding width in bins of 0.25 μm size. The number of spines in each bin was then divided by the total number analyzed. The resulting percentages gave the heights of the intersections of the grid. Then, horizontal "isofrequency" lines of equal percentage separated by different colors were added. Statistical significance was determined by Student's t test.

Whole-Cell Recording

Rat hippocampal neurons were cultured as described previously (Liu and Tsien, 1995) and transfected at DIV5–6 with GFP or GFP + Shank, using calcium phosphate precipitation. Whole-cell recordings were obtained at room temperature (23°C–25°C) from GFP-fluorescent spindle-shaped pyramidal neurons at DIV11 or 17. Cells were recorded while in Tyrode's solution containing (in mM) NaCl, 124; KCl, 5; $CaCl_2$, 2; $MgCl_2$, 1; glucose, 30; and HEPES, 25 (pH 7.4 with NaOH). Tetradotoxin (1 μm) and picrotoxin (50 μm) were added to block action potentials and GABAergic transmission. The recordings were made with an Axon Instruments model 200B integrating patch-clamp amplifier with a 1 kHz Bessell low-pass filter. Miniature EPSCs were detected by custom software using a template matching algorithm (Clements and Bekkers, 1997). Once all mEPSCs were located, their peak amplitudes and intervals were calculated.

Functional Imaging with GFP and FM4-64

GFP and FM dye signals were imaged using an Olympus 40× water immersion objective. The staining procedure for FM4-64 is similar to FM1-43 (Liu et al., 1999). To quantify the FM uptake by synapses on GFP-positive cells, the boundaries of transfected cells were first defined by GFP fluorescence. Individual FM spots occurring within this outlined area were selected using ImageTool 2.0 (UTHSCSA, San Antonio, TX), and the number of FM puncta per unit area (μm^2) of GFP was counted. FM puncta were discerned from "background," based on a manually selected threshold, which biases against puncta of too small an area or too low brightness. Thus, differences quantified under this method could reflect an increase in the number of functional synapses and/or a general enlargement of functional vesicle pool size such that more synapses meet the threshold.

Acknowledgments

We are grateful to Eunjoon Kim and Scott Naisbitt for helpful discussions; Sheila Rudolph-Correia and Bing Li for technical assistance; Eunjoon Kim for Homer and guinea pig Shank antibodies; Paul Worley for Myc-Homer1b cDNA; and Craig Garner for Bassoon antibodies. C.S. was supported by the Harvard-Armenise Foundation (Department of Biological and Technical Research [DIBIT], Hospital San Raffaele, Scientific Institute, San Raffaele, Italy). M.S. is an Assistant Investigator of the Howard Hughes Medical Institute.

Received October 31, 2000; revised April 24, 2001.

References

Bailey, C.H., and Kandel, E.R. (1993). Structural changes accompanying memory storage. Annu. Rev. Physiol. *55*, 397–426.

Boeckers, T.M., Kreutz, M.R., Winter, C., Zuschratter, W., Smalla, K.H., Sanmarti-Vila, L., Wex, H., Langnaese, K., Bockmann, J., Garner, C.C., et al. (1999a). Proline-rich synapse-associated protein-1/cortactin binding protein 1 (ProSAP1/CortBP1) is a PDZ-domain protein highly enriched in the postsynaptic density. J. Neurosci. *19*, 6506–6518.

Boeckers, T.M., Winter, C., Smalla, K.H., Kreutz, M.R., Bockmann, J., Seidenbecher, C., Garner, C.C., and Gundelfinger, E.D. (1999b). Proline-rich synapse-associated proteins ProSAP1 and ProSAP2 interact with synaptic proteins of the SAPAP/GKAP family. Biochem. Biophys. Res. Commun. *264*, 247–252.

Brewer, G.J., Torricelli, J.R., Evege, E.K., and Price, P.J. (1993). Optimized survival of hippocampal neurons in B27-supplemented Neurobasal, a new serum-free medium combination. J. Neurosci. Res. *35*, 567–576.

Calverley, R.K., and Jones, D.G. (1990). Contributions of dendritic spines and perforated synapses to synaptic plasticity. Brain Res. Brain Res. Rev. *15*, 215–249.

Clements, J.D., and Bekkers, J.M. (1997). Detection of spontaneous synaptic events with an optimally scaled template. Biophys. J. *73*, 220–229.

Desmond, N.L., and Levy, W.B. (1988). Synaptic interface surface area increases with long-term potentiation in the hippocampal dentate gyrus. Brain Res. *453*, 308–314.

Du, Y., Weed, S.A., Xiong, W.-C., Marshall, T.D., and Parsons, J.T. (1998). Identification of a novel Cortactin SH3 domain-binding protein and its localization to growth cones of cultured neurons. Mol. Cell. Biol. *18*, 5838–5851.

Ehlers, M.D. (1999). Synapse structure: glutamate receptors connected by the shanks. Curr. Biol. *9*, R848–R850.

El-Husseini, A.E., Schnell, E., Chetkovich, D.M., Nicoll, R.A., and Bredt, D.S. (2000). PSD-95 involvement in maturation of excitatory synapses. Science *290*, 1364–1368.

Engert, F., and Bonhoeffer, T. (1999). Dendritic spine changes associated with hippocampal long-term synaptic plasticity. Nature *399*, 66–70.

Fifkova, E., and Van Harreveld, A. (1977). Long-lasting morphological changes in dendritic spines of dentate granular cells following stimulation of the entorhinal area. J. Neurocytol. *6*, 211–230.

Fischer, M., Kaech, S., Knutti, D., and Matus, A. (1998). Rapid actin-based plasticity in dendritic spines. Neuron *20*, 847–854.

Garner, C.C., Nash, J., and Huganir, R.L. (2000). PDZ domains in synapse assembly and signalling. Trends Cell. Biol. *10*, 274–280.

Harris, K. (1999a). Structure, development, and plasticity of dendritic spines. Curr. Opin. Neurobiol. *9*, 343–348.

Harris, K.M. (1999b). Calcium from internal stores modifies dendritic spine shape. Proc. Natl. Acad. Sci. USA *96*, 12213–12215.

Harris, K., and Kater, S. (1994). Dendritic spines: cellular specializations imparting both stability and flexibility to synaptic function. Annu. Rev. Neurosci. *17*, 341–371.

Horner, C.H. (1993). Plasticity of the dendritic spine. Prog. Neurobiol. *41*, 281–321.

Hosokawa, T., Rusakov, D.A., Bliss, T.V., and Fine, A. (1995). Repeated confocal imaging of individual dendritic spines in the living hippocampal slice: evidence for changes in length and orientation associated with chemically induced LTP. J. Neurosci. *15*, 5560–5573.

Kennedy, M.B. (1997). The postsynaptic density at glutamatergic synapses. Trends Neurosci. *20*, 264–268.

Kim, E., Naisbitt, S., Hsueh, Y.-P., Rao, A., Rothschild, A., Craig, A.M., and Sheng, M. (1997). GKAP, a novel synaptic protein that interacts with the guanylate kinase-like domain of the PSD-95/SAP90 family of channel clustering molecules. J. Cell Biol. *136*, 669–678.

Korkotian, E., and Segal, M. (1999). Release of calcium from stores alters the morphology of dendritic spines in cultured hippocampal neurons. Proc. Natl. Acad. Sci. USA *96*, 12068–12072.

Kreienkamp, H.J., Zitzer, H., Gundelfinger, E.D., Richter, D., and Bockers, T.M. (2000). The calcium-independent receptor for alpha-latrotoxin from human and rodent brains interacts with members of the ProSAP/SSTRIP/Shank family of multidomain proteins. J. Biol. Chem. *275*, 32387–32390.

Lim, S., Naisbitt, S., Yoon, J., Hwang, J.I., Suh, P.G., Sheng, M., and Kim, E. (1999). Characterization of the Shank family of synaptic proteins. Multiple genes, alternative splicing, and differential expression in brain and development. J. Biol. Chem. *274*, 29510–29518.

Liu, G., and Tsien, R.W. (1995). Properties of synaptic transmission at single hippocampal synaptic boutons. Nature *375*, 404–408.

Liu, G., Choi, S., and Tsien, R.W. (1999). Variability of neurotransmitter concentration and nonsaturation of postsynaptic AMPA receptors at synapses in hippocampal cultures and slices. Neuron *22*, 395–409.

Maletic-Savatic, M., Malinow, R., and Svoboda, K. (1999). Rapid dendritic morphogenesis in CA1 hippocampal dendrites induced by synaptic activity. Science *283*, 1923–1927.

Matus, A., Brinkhaus, H., and Wagner, U. (2000). Actin dynamics in dendritic spines: a form of regulated plasticity at excitatory synapses. Hippocampus *10*, 555–560.

Muller, D., Toni, N., and Buchs, P.A. (2000). Spine changes associated with long-term potentiation. Hippocampus *10*, 596–604.

Naisbitt, S., Kim, E., Tu, J.C., Xiao, B., Sala, C., Valtschanoff, J., Weinberg, R.J., Worley, P.F., and Sheng, M. (1999). Shank, a novel family of postsynaptic density proteins that binds to the NMDA receptor/PSD-95/GKAP complex and cortactin. Neuron *23*, 569–582.

Nakayama, A.Y., Harms, M.B., and Luo, L. (2000). Small GTPases Rac and Rho in the maintenance of dendritic spines and branches in hippocampal pyramidal neurons. J. Neurosci. *20*, 5329–5338.

Renger, J.J., Egles, C., and Liu, G. (2001). A developmental switch in neurotransmitter flux enhances synaptic efficacy by affecting AMPA receptor activation. Neuron *29*, 469–484.

Rusakov, D.A., Richter-Levin, G., Stewart, M.G., and Bliss, T.V. (1997). Reduction in spine density associated with long-term potentiation in the dentate gyrus suggests a spine fusion-and-branching model of potentiation. Hippocampus *7*, 489–500.

Sala, C., Rudolph-Correia, S., and Sheng, M. (2000). Developmentally regulated NMDA receptor-dependent dephosphorylation of cAMP response element-binding protein (CREB) in hippocampal neurons. J. Neurosci. *20*, 3529–3536.

Sheng, M., and Kim, E. (2000). The Shank family of scaffold proteins. J. Cell Sci. *113*, 1851–1856.

Sheng, M., and Pak, D.T.S. (2000). Ligand-gated ion channel interactions with cytoskeletal and signaling proteins. Annu. Rev. Physiol. *62*, 755–778.

Shiraishi, Y., Mizutani, A., Bito, H., Fujisawa, K., Narumiya, S., Mikoshiba, K., and Furuichi, T. (1999). Cupidin, an isoform of Homer/Vesl, interacts with the actin cytoskeleton and activated rho family small GTPases and is expressed in developing mouse cerebellar granule cells. J. Neurosci. *19*, 8389–8400.

Spacek, J., and Harris, K. (1997). Three-dimensional organization of smooth endoplasmic reticulum in hippocampal CA1 dendrites and dendritic spines of the immature and mature rat. J. Neurosci. *17*, 190–203.

Steward, O., and Schuman, E.M. (2001). Protein synthesis at synaptic sites on dendrites. Annu. Rev. Neurosci. *24*, 299–325.

Tobaben, S., Sudhof, T.C., and Stahl, B. (2000). The G protein-coupled receptor CL1 interacts directly with proteins of the Shank family. J. Biol. Chem. *46*, 36204–36210.

Toni, N., Buchs, P.A., Nikonenko, I., Bron, C.R., and Muller, D. (1999). LTP promotes formation of multiple spine synapses between a single axon terminal and a dendrite. Nature *402*, 421–425.

Tu, J.C., Xiao, B., Yuan, J.P., Lanahan, A.A., Leoffert, K., Li, M., Linden, D.J., and Worley, P.F. (1998). Homer binds a novel proline-rich motif and links group 1 metabotropic glutamate receptors with IP3 receptors. Neuron *21*, 717–726.

Tu, J.C., Xiao, B., Naisbitt, S., Yuan, J.P., Petralia, R.S., Brakeman, P., Doan, A., Aakalu, V.K., Lanahan, A.A., Sheng, M., et al. (1999). Coupling of mGluR/Homer and PSD-95 complexes by the Shank family of postsynaptic density proteins. Neuron *23*, 583–592.

Valtschanoff, J.G., and Weinberg, R.J. (2001). Laminar organization of the NMDA receptor complex within the postsynaptic density. J. Neurosci. *21*, 1211–1217.

Weed, S.A., Du, Y., and Parsons, J.T. (1998). Translocation of cortactin to the cell periphery is mediated by the small GTPase Rac1. J. Cell Sci. *111*, 2433–2443.

Xiao, B., Tu, J.C., Petralia, R.S., Yuan, J.P., Doan, A., Breder, C.D., Ruggiero, A., Lanahan, A.A., Wenthold, R.J., and Worley, P.F. (1998). Homer regulates the association of group 1 metabotropic glutamate receptors with multivalent complexes of homer-related, synaptic proteins. Neuron *21*, 707–716.

Xiao, B., Tu, J.C., and Worley, P.F. (2000). Homer: a link between neural activity and glutamate receptor function. Curr. Opin. Neurobiol. *10*, 370–374.

Yao, I., Hata, Y., Hirao, K., Deguchi, M., Ide, N., Takeuchi, M., and Takai, Y. (1999). Synamon, a novel neuronal protein interacting with synapse-associated protein 90/postsynaptic density-95-associated protein. J. Biol. Chem. *274*, 27463–27466.

Ziff, E.B. (1997). Enlightening the postsynaptic density. Neuron *19*, 1163–1174.

Zitzer, H., Honck, H.H., Bachner, D., Richter, D., and Kreienkamp, H.J. (1999a). Somatostatin receptor interacting protein defines a novel family of multidomain proteins present in human and rodent brain. J. Biol. Chem. *274*, 32997–33001.

Zitzer, H., Richter, D., and Kreienkamp, H.J. (1999b). Agonist-dependent interaction of the rat somatostatin receptor subtype 2 with cortactin-binding protein 1. J. Biol. Chem. *274*, 18153–18156.